

# **A novel sensing platform based on Polyglycine-Modified CVD Graphene for the Simultaneous Determination of Dopamine, Uric Acid, Guanine and Adenine**

*Yitao Zhang, Ziwei Wang, Hongxia Luo\**

Department of Chemistry, Renmin University of China, Beijing 100872, China

\*E-mail: [luohx@ruc.edu.cn](mailto:luohx@ruc.edu.cn)

*Received: 25 June 2020 / Accepted: 26 August 2020 / Published: 30 September 2020*

---

A novel strategy based on a free-standing graphene platform electrode (GPE) incorporating polymerized glycine (poly-Gly) was proposed to simultaneously discriminate dopamine (DA), uric acid (UA), guanine (G) and adenine (A). Graphene film grown by chemical vapor deposition (CVD) was diverted onto polyethylene terephthalate (PET) under the support of polymer. Subsequently, GPE was successfully constructed by immersing the composite in acetone to remove the polymer. Gly was anchored on the platform to obtain poly-Gly/GPE by performing a simple electropolymerization technique. The proposed electrode exhibited high selectivity and excellent electrocatalytic activities to discriminate the four biomolecules. The potential differences of DA-UA, UA-G and G-A were 160, 400 and 315 mV, respectively.

---

**Keywords:** CVD graphene; Glycine; Electrochemical sensing

## **1. INTRODUCTION**

As the most abundant catecholamine neurotransmitter in the brain, dopamine (DA) regulates and controls many physiological functions of the central nervous system [1]. The dysregulation of dopamine involves pituitary tumours, neurosis, etc. [2] As a main metabolite of birds and reptiles, uric acid (UA) has been paid increasingly attention.[3]. Urine of a normal human body contains a small amount of uric acid [4]. The rate of production and excretion of uric acid in a normal human body is basically constant [5]. The change in uric acid content in body fluid can fully reflect the metabolism, immunity and other functions of the human body [6]. Guanine (G) is an organic purine compound and has crucial physiological function with extremely low content in organism [7]. Adenine (A) is a nitrogen-containing heterocyclic derivative. Adenine and its derivatives have various biochemical functions. G and A are among the five main nitrogenous bases in deoxyribonucleic acid and ribonucleic acid [8]. If the

concentration of G and A is abnormal, it may indicate a defect or mutation of the human immune system [9]. Since they generally coexist in biological samples, a feasible technique to simultaneously discriminate these four compounds is crucial. [10-14].

Several reports had realized the discrimination of these four biomolecules. To simultaneously discriminate UA, ascorbic acid (AA) and DA, Sheng et al. utilized a nitrogen-doped graphene sensor to achieve the goal. [15]. Yin et al. used an electrode incorporating Nafion–graphene composite film to concurrently detect G and A [16]. He et al. prepared a polyglycine/graphene oxide modified electrode to individually and simultaneously electrochemically discriminate UA, DA, A and G [11]. Niu et al. prepared a DNA/nano-Au composite biosensor, which was applied to sensitively concurrently discriminate UA, DA, A and G [13]. Liu et al. reported an electrode assembled with graphene oxide/polyimidazole co-macromolecule to concurrently discriminate UA, DA, A, G and AA [12].

Graphene, which is a flexible plane, is one of the most outstanding two-dimensional carbon materials [17]. Due to its fast electron transfer capability and relative huge specific area, graphene has become upsurge in both fundamental and application fields such as electrochemical sensors, batteries [18], super capacitors and fuel cells [19, 20]. Nowadays, there are two conventional methods to fabricate graphene electrodes: coating graphene homogeneous suspension droplets [21] and reducing graphene oxide (ERGO) by electrochemical reduction after the self-assembly of graphene oxide (GO) [22]. Unfortunately, the reproducibility obtained by these methods is poor because of their lack of control over the graphene content and thickness of graphene films. Chemical-vapor-deposited (CVD) graphene exhibits excellent properties due to its controllable film thickness and fewer structural defects on the surface [23]. Through the controllable deposition process, the uniform graphene film has clear layers [24].

There are two types of CVD graphene: edge plane and basal plane with significant electrochemical performance [25]. In our previous work, graphene film was applied to fabricate a linear edge nanoelectrode to detect biomolecules [26]. A non-enzymatic biosensor for glucose was constructed by depositing Cu nanoparticles on the edge. [27]. Meanwhile, a graphene platform electrode (GPE) was constructed by diverting graphene film onto polyethylene terephthalate (PET) under the support of polymer [28]. GPE incorporating L-cysteine as a sensor was fabricated to simultaneously discriminate AA and DA [28]. On this basis, L-cysteine and AuPt hybrid nanoparticles were deposited on the platform to construct AuPtNPs-Cys/GPE, which was utilized to selectively discriminate epinephrine [24]. In addition, tyrosine, acetaminophen and epinephrine were simultaneously detected by electrodepositing L-aspartic acid on GPE [29]. In the present work, glycine (Gly) was electro-polymerized on the platform to prepare poly-Gly/GPE. The as-obtained poly-Gly/GPE was appropriately utilized to simultaneously discriminate UA, DA, A and G under interference of EP and AA in certain concentrations. Fig. 1 shows the complete fabrication, detection and analysis process.

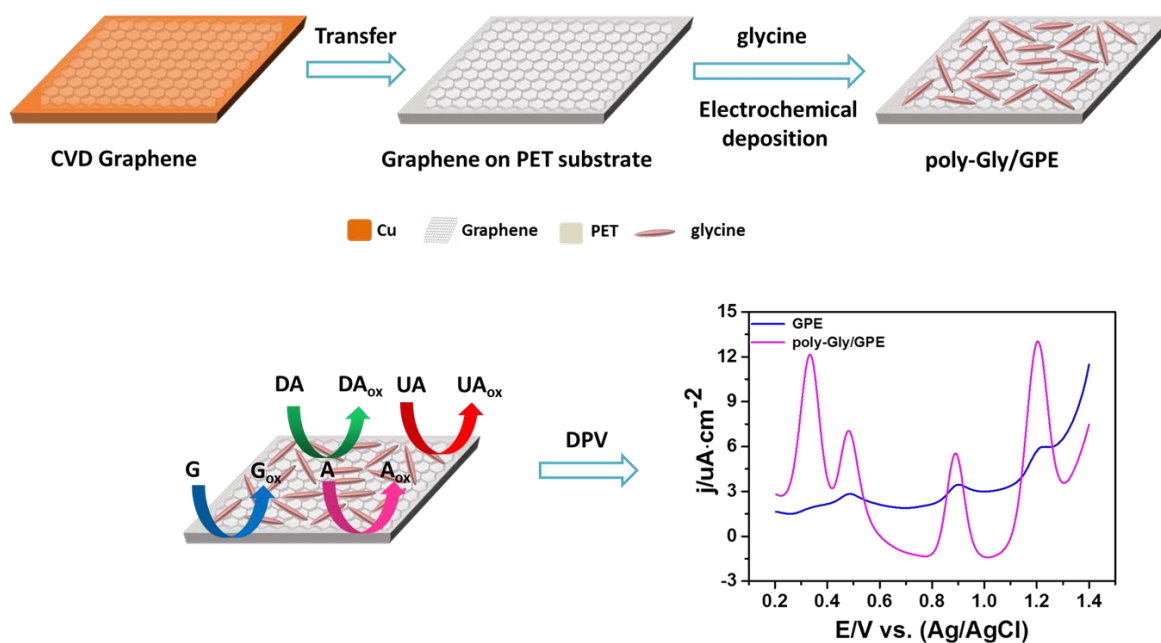


**Figure 1.** Fabrication, detection and analysis process of poly-Gly/GPE.

## 2. EXPERIMENT

### 2.1. Preparation of GPE

Figure 2 shows the entire preparation process. The few-layer high-quality large-area graphene was diverted onto PET by a nondestructive polymer-supported transfer method [30]. First, the front side of the CVD graphene film was coated on 2% PMMA (anisole as solvent) and stand for a while to volatilize anisole. Then, the composite was dried at 115 °C for 10 min to form a PMMA/graphene/copper/graphene sheet [31]. Second, to remove useless graphene layers and corrode copper foils, the opposite side was polished and floated face up on an FeCl<sub>3</sub> solution for 30 min [24]. After FeCl<sub>3</sub> was completely cleared, it was repeatedly washed by distilled water [28]. Then, the PMMA/graphene film was supported by a PET sheet and dried at room temperature overnight to ensure that the graphene film tightly adhered on PET [29]. To remove the upper layer of PMMA, it was fully immersed in acetone for 20 hours to ensure that acetone was absolutely cleared; then, it was removed to dry. [24]. Finally, graphene/PET was cut into strips and wrapped in insulating tape to control the working area [28]. The electrode and electrochemical instrument were connected through the copper tape.

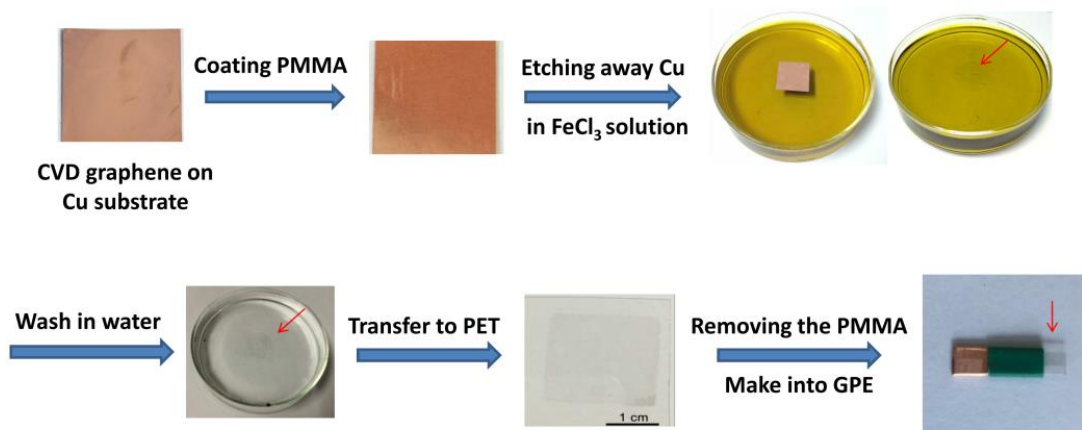


**Figure 2.** Constructing a graphene platform electrode.

## 2.2. Modification of GPE

The electro-deposition of Gly was performed by cyclic voltammetry (CV): In 5 mM gly with 0.1 M PBS (pH 4.0), Gly was electro-polymerized on the graphene platform by scanning 25 cycles at 50 mV from -0.6 V to 1.4 V. Then, poly-Gly/GPE was washed three times and dried. To obtain a stable voltammogram for the blank control, the prepared poly-Gly/GPE was scanned several cycles in blank PBS (pH 4.0) in the potential window of measurement of 0.0 - 1.5 V.

## 3. RESULTS AND DISCUSSION

### 3.1. Characterization

Fig. 3 illustrates the graphene film at different transfer stages recorded by scanning electron microscopy (SEM). Fig. 3A reveals a smooth surface of the graphene sheet on Cu. Fig. 3B shows that graphene (on PET) retained a very good continuity, which certifies that the graphene film was successfully transferred. Fig. 3C shows that stick-like Gly was firmly anchored on the graphene platform.

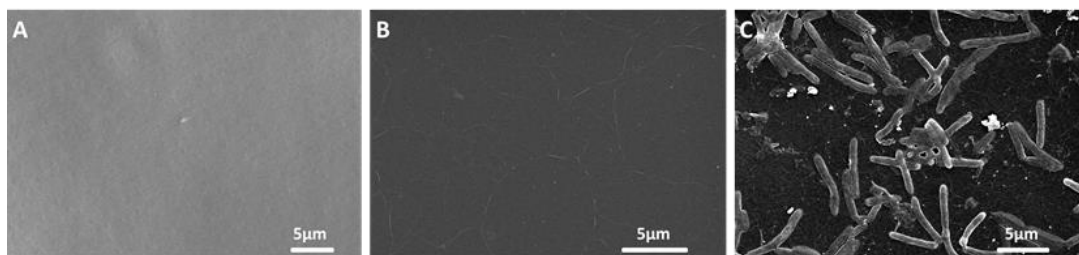


**Figure 3.** (A-B) SEM image of graphene on Cu and PET; (C) SEM images of poly-Gly/GPE

As a powerful technique to characterize structures, Raman spectroscopy was generally applied to identify the structure of the graphene film, including the chemical groups and defect degree. [32] The

Raman spectra of graphene on Cu (black) and PET (red) were recorded (Fig. 4). Two obvious peaks were utilized to characterize CVD graphene film: G band ( $1579\text{ cm}^{-1}$ ) and 2D band ( $2697\text{ cm}^{-1}$ ) [33]. As a parameter to characterize the number of layers and thickness of the film, the ratio of G and 2D bands proves that the graphene film had few layers, and the thickness was nano-scale [34]. The defect intensity was studied using the D band at  $1346\text{ cm}^{-1}$ . The D band was only a small peak, which shows that the graphene film was almost intact. The Raman spectra of graphene on Cu (black) was almost identical to that on PET (red), which validates that the transfer process was high-quality.

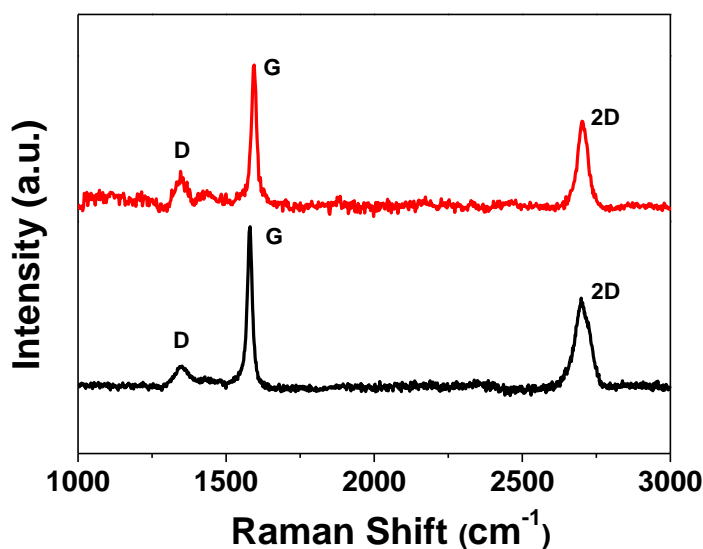


**Figure 4.** Raman spectra of graphene on PET (red) and Cu (black)

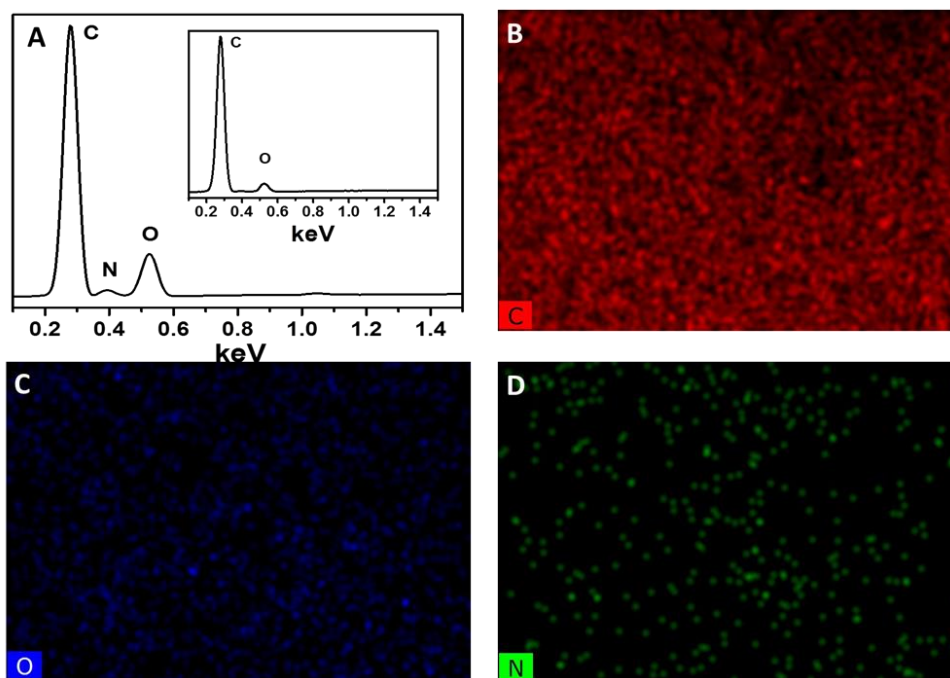


**Figure 5.** (A) EDS spectra and (B-D) element surface distribution of poly-Gly/GPE.

To verify whether Gly was polymerized on the electrode surface, the energy dispersive spectrometer (EDS) was used. As shown in Fig. 5A, a slight peak of N element appeared compared to the bare GPE (inset of Fig. 5A) due to the modification of Gly. The oxygen-to-carbon ratio increased from bare GPE to poly-Gly/GPE, which suggests that some carbon atoms on the graphene platform were oxidized. The oxidation on the surface increased the catalytic activities for biomolecules, which also significantly improved the electrode performance. [35]. Element mapping (Fig. 5B-D) preferably proves that Gly was successfully anchored on the platform of the electrode.

Fig. 6 shows the electrochemical impedance spectra (EIS) of poly-Gly/GPE and GPE. The Randle circuit (Fig. 6) was selected to equate the obtained data of impedance. The decrease in  $R_{ct}$  after modification shows that the modified Gly on the electrode surface promoted the efficiency of electron transmission. Thus, the current signal of poly-Gly/GPE remarkably increased compared to that of the bare GPE.

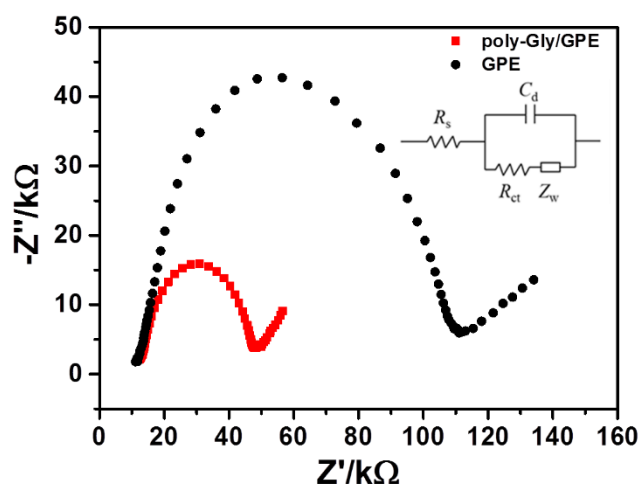


**Figure 6.** Nyquist plots of poly-Gly/GPE and GPE in 1 mM  $[\text{Fe}(\text{CN})_6]^{3-/4-}$  solution with 0.1 M KCl.

### 3.2. Electrochemical performance

To investigate the electro-chemical characteristics of GPE and poly-Gly/GPE, CV and differential pulse voltammogram (DPV) were performed. Fig. 7A shows the CV of poly-Gly/GPE and GPE in the presence of the four biomolecules. No signal was observed at two electrodes in the blank buffer solution (red, black curve), which suggested that both electrodes had sufficiently clear surfaces with no electro-active material. Four slight electrochemical signals appeared at bare GPE in the presence of the four biomolecules in PBS (pH 4.0) (blue curve). After modification, four oxidation peaks significantly improved at poly-Gly/GPE (magenta curve), and their shape became sharp compared to bare GPE. The peak separation ( $\Delta E_p$ ) between DA and UA was 160 mV due to the negative shift of the DA peak potential, which enabled the simultaneous discrimination of UA and DA. The DPV results (Fig. 7B) at GPE (blue curve) and poly-Gly/GPE (magenta curve) were consistent with CV.

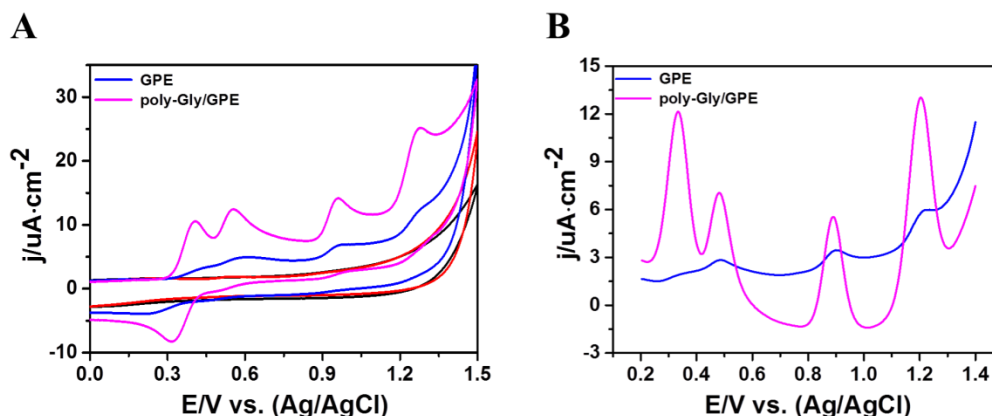


**Figure 7.** (A) CV measured by GPE and poly-Gly/GPE in the presence (blue/magenta) and absence (red/black) of 50  $\mu\text{M}$  DA, 40  $\mu\text{M}$  UA, 25  $\mu\text{M}$  G and 30  $\mu\text{M}$  A with 0.1 M PBS (pH 4.0); (B) DPV measured by GPE (blue) and poly-Gly/GPE (magenta) in the presence of 50  $\mu\text{M}$  DA, 40  $\mu\text{M}$  UA, 25  $\mu\text{M}$  G and 30  $\mu\text{M}$  A with 0.1 M PBS (pH 4.0).

### 3.3. Optimization of parameters

#### 3.3.1. Electro-deposition cycle number

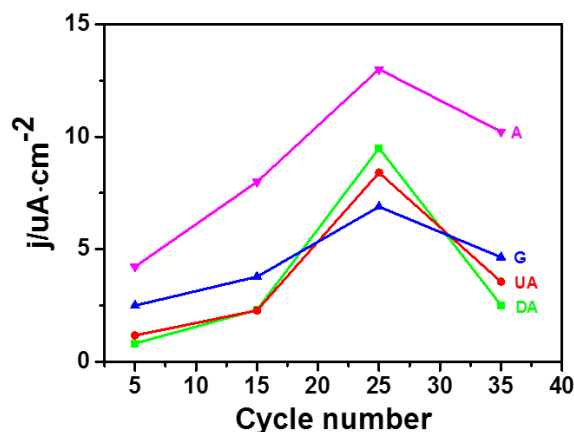


**Figure 8.** Current density vs. cycle number of electropolymerization.

To study the dependence between current density and cycle number of electro-deposition, the DPV method was performed in the presence of 50  $\mu\text{M}$  DA, 40  $\mu\text{M}$  UA, 25  $\mu\text{M}$  G and 30  $\mu\text{M}$  A with 0.1 M PBS (pH 4.0). As shown in Fig. 8, below 25 cycles, the signal intensity increased with the cycle number. When the cycle number exceeded 25, which corresponded to the maximum current density, the current density obviously decreased when the cycle number increased. This result might be attributed to the saturated occupation of the electro-catalytic site at 25 cycles. Excessive electro-deposition cycles would form a too thick film on graphene, which would hinder the electron transfer on the electrode surface.

### 3.3.2. pH value

To select a suitable pH value to simultaneously discriminate the four compounds based on poly-Gly/GPE, the DPV method was performed with various pH values (Fig. 9A). Fig. 9B presents the dependence between peak potential and pH. The peak potentials of four biomolecules positively shifted when pH continued decreasing. These phenomena suggest that protons combined with oxidation products during the reaction. There was no remarkable distinction in peak potential interval of four compounds under various pH values, where all peak potential intervals of DA-UA were approximately 160 mV. The oxidation peak potentials of all the biomolecules were found to be proportional linearly to the pH values (Fig. 9B). And the slopes of the linear regression lines were all approached the theoretical value ( $59 \text{ mV pH}^{-1}$ ), which proved that an equivalent number of electrons and protons were involved in the oxidation process of the four biomolecules. [36].

In Fig. 9C, with increasing pH value, the current signals of A and G decreased. The maximum current signals of UA and DA occurred at pH = 4.0. In summary, the best environmental condition of pH was selected as 4.0 for further experiments.

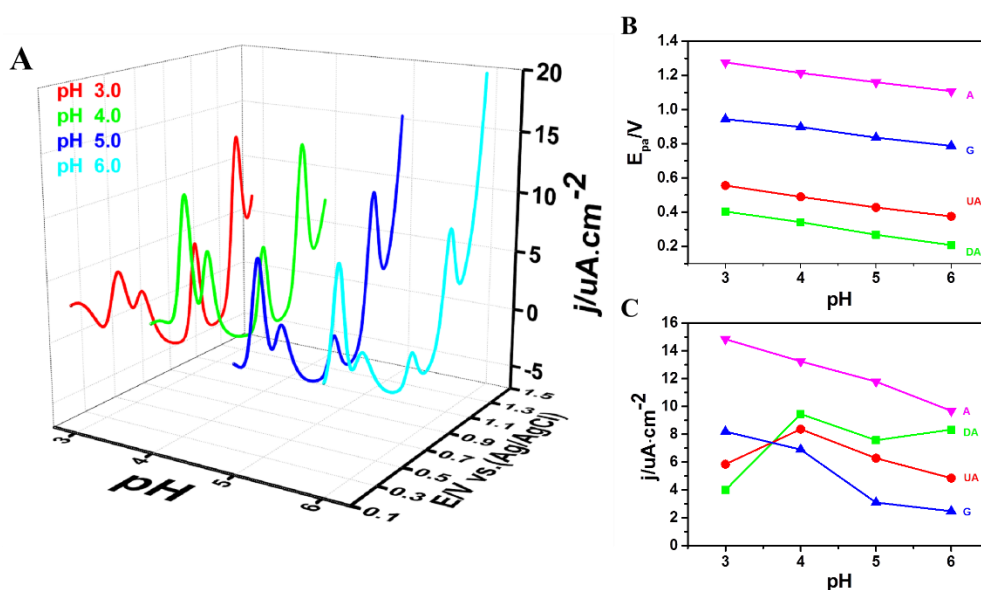


**Figure 9.** (A) DPVs of 50  $\mu\text{M}$  DA, 40  $\mu\text{M}$  UA, 25  $\mu\text{M}$  G and 30  $\mu\text{M}$  A on poly-Gly/GPE with various pH (3.0-6.0); (B) Regression function between peak potential and pH. (C) Dependence between current density and pH.

### 3.3.3. Scan rate

CV was performed at 10-310 mV/s to study the electro-chemical behaviour of the four biomolecules (Fig. 10A). Fig. 10B depicts the linear relationships between the current density of the four biomolecules and the square root of the scan rate. According to the electrode reaction kinetics, if the current is linear with the square root of the scan rate, the reaction rate is controlled by diffusion [37]. Hence, the reactions of the four species on poly-Gly/GPE were diffusion-controlled processes.

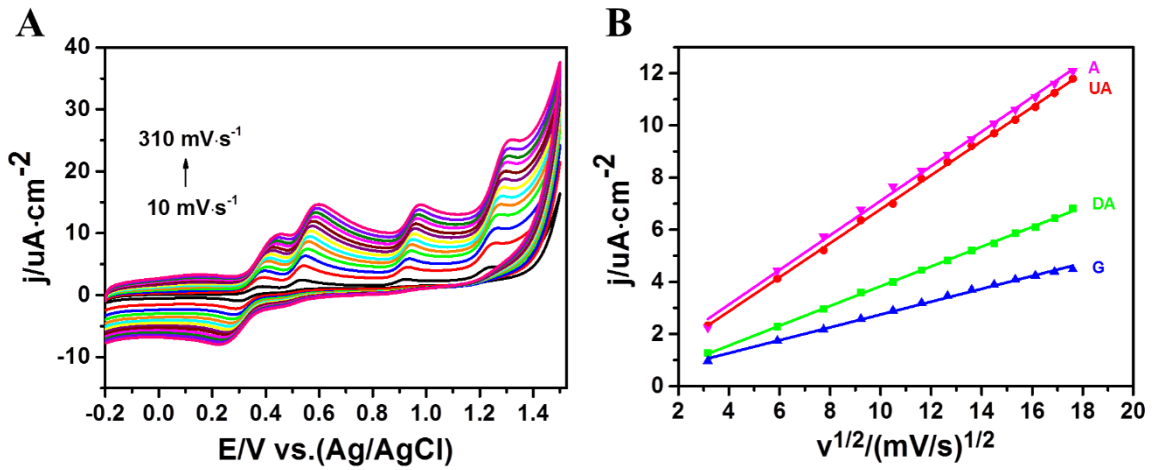


**Figure 10.** (A) CVs obtained from 20  $\mu\text{M}$  DA, 15  $\mu\text{M}$  UA, 10  $\mu\text{M}$  G and 15  $\mu\text{M}$  A at various scan rates (10 - 310 mV/s); (B)  $j/(\mu\text{A} \cdot \text{cm}^{-2})$  vs.  $v^{1/2}(\text{mV/s})^{1/2}$ .

### 3.4. Simultaneous and individual determination of DA, UA, G and A

Fig. 11 displays the DPV obtained by concurrently changing the concentration of four substances in the mixture at poly-Gly/GPE. The peaks of the four substances were segregated at various concentrations, and the current signals of the four substances linearly magnified with the simultaneous increase in concentration.

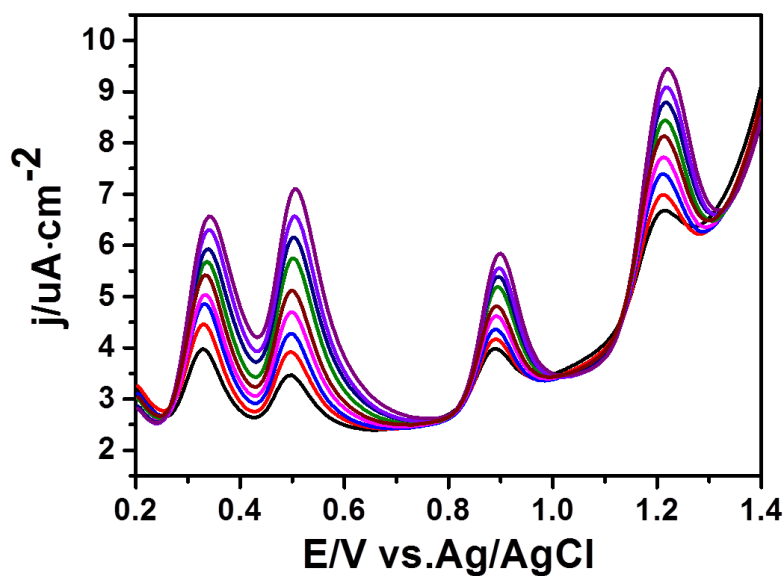


**Figure 11.** DPV obtained from DA, UA, G and A at various concentrations on poly-Gly/GPE in 0.1 M PBS (pH 4.0).

To testify that the as-prepared electrode can simultaneously detect four biomolecules using the DPV measurement method, individual detections were investigated. In other words, the concentration of one biomolecule was increased in the mixture when the other three remained unchanged, and the magnification of the current signal intensity was recorded during the entire process (Fig. 12).

The linear fitting equations of the individual detection of four biomolecules were as follows:

$$j \text{ (DA)} (\mu\text{A}\cdot\text{cm}^{-2}) = 0.1777 C_{\text{DA}} (\mu\text{M}) + 0.2056 \text{ (R}^2 = 0.9998) \text{ (Fig. 12A)}$$

$$j \text{ (UA)} (\mu\text{A}\cdot\text{cm}^{-2}) = 0.1889 C_{\text{UA}} (\mu\text{M}) + 0.5441 \text{ (R}^2 = 0.9978) \text{ (Fig. 12B)}$$

$$j \text{ (G)} (\mu\text{A}\cdot\text{cm}^{-2}) = 0.2462 C_{\text{G}} (\mu\text{M}) + 0.3411 \text{ (R}^2 = 0.9993) \text{ (Fig. 12C)}$$

$$j \text{ (A)} (\mu\text{A}\cdot\text{cm}^{-2}) = 0.4161 C_{\text{A}} (\mu\text{M}) + 0.5694 \text{ (R}^2 = 0.9980) \text{ (Fig. 12D)}$$

Their limits of detection (LODs) were 0.089  $\mu\text{M}$ , 0.10  $\mu\text{M}$ , 0.039  $\mu\text{M}$ , and 0.033  $\mu\text{M}$  (S/N=3) with the linear ranges of 0.30-60  $\mu\text{M}$ , 0.40-105  $\mu\text{M}$ , 0.15-37  $\mu\text{M}$ , and 0.10-56  $\mu\text{M}$ , respectively.

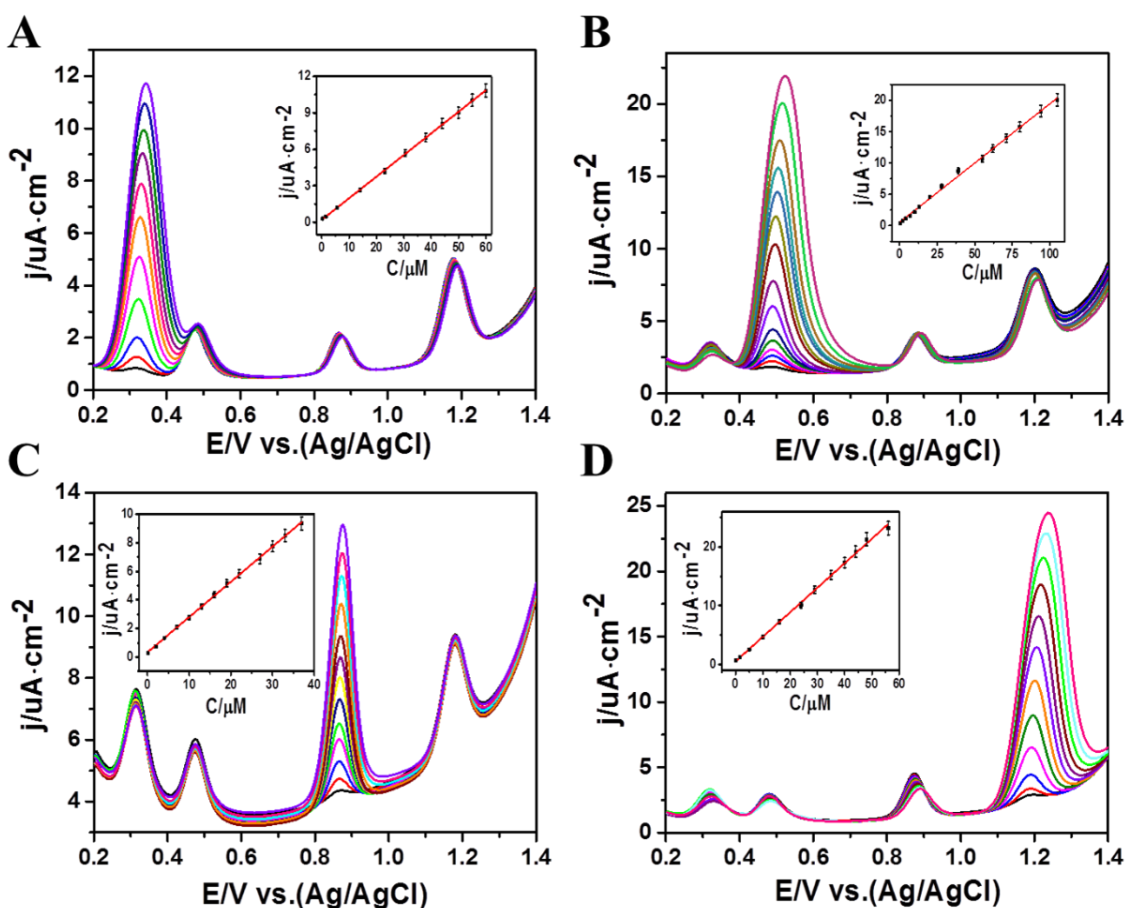


**Figure 12.** (A) DPV at poly-Gly/GPE of DA with various concentrations in the mixture (pH 4.0) ; (B) DPV at poly-Gly/GPE of UA with various concentrations in the mixture (pH 4.0) at poly-Gly/GPE; (C) DPV at poly-Gly/GPE of G with various concentrations in the mixture (pH 4.0) at poly-Gly/GPE; (D) DPV at poly-Gly/GPE of A with various concentrations in the mixture (pH 4.0) at poly-Gly/GPE.

## 3.5. Interference studies

A mixture of four biomolecules and potential disruptors, which contained 50 mM  $\text{NH}_4^+$ ,  $\text{Cl}^-$ ,  $\text{SO}_4^{2-}$ ,  $\text{NO}_3^-$ , 5 mM citric acid (CA), glucose (Glu), tryptophan (Trp), 50  $\mu\text{M}$  epinephrine (EP), and ascorbic acid (AA), was successively added to the aqueous solution (pH 4.0) and recorded by Chronoamperometry (Fig. 13). No new signal was detected when eight interfering species were added into the solution. However, when another target analyte was added, a strong current signal accompanying a step immediately appeared. These results show that the as-prepared electrode had good anti-interference performance and excellent selectivity in the non-enzymatic electro-catalysis

**Table 1.** Comparison of the major characteristics of various biosensors.

Biosensors	Linear range ( $\mu\text{M}$ )				Detection limit ( $\mu\text{M}$ )				Ref
	DA	UA	G	A	DA	UA	G	A	
Ag-PMel/GCE	0.10-50	0.10-50	0.10-50	0.10-60	0.010	0.10	0.0080	0.0080	[14]
AuNPs/DNA/AuNPs/poly(SFR)/GCE	0.0080-1.1	0.090-12	0.0090-5.0	0.060-0.80	0.00020	0.0080	0.00050	0.0040	[13]
NiFe/C/GCE	0.50-130	0.25-110	1.0-200	1.0-200	0.10	0.10	0.25	0.25	[38]
NiCu/C/GCE	0.25-40	0.50-110	0.50-480	0.50-450	0.010	0.050	0.10	0.10	[39]
P-GLY/GO/GCE	0.20-62	0.10-105	0.15-48	0.090-103	0.011	0.061	0.026	0.030	[11]
Plmox/GO/GCE	12-278	3.6-249.6	3.3-103.3	9.6-215	0.63	0.59	0.48	1.28	[12]
Au/HGE	0.4-20	0.6-40	6-500	0.6-40	0.02	0.57	2.5	0.42	[10]
Ag-PMel/GCE	0.1-50	0.1-50	0.1-50	0.1-60	0.01	0.1	0.008	0.008	[40]
Graphene-4	0.1-10	0.2-10	3-100	0.1-10	0.001	0.002	0.2	0.0015	[41]
	10-40	10-50	100-700	10-70					
T-Ag@Cu <sub>2</sub> O@GO/GCE	0.0005-0.0010	0.0060-0.050	0.0010-0.0020	0.0060-0.020	0.00010	0.0060	0.00020	0.0030	[42]
FeTe <sub>2</sub> /GP	5-120	3-120	1-160	3-100	0.028	0.042	0.034	0.026	[43]
Fe <sub>3</sub> O <sub>4</sub> @NHCS/GCE	0.01-40	0.10-40	0.50-30	0.50-40	0.0063	0.0361	0.1432	0.1235	[44]
poly-Gly/GPE	0.3-60	0.4-105	0.15-37	0.10-56	0.089	0.10	0.039	0.033	This work

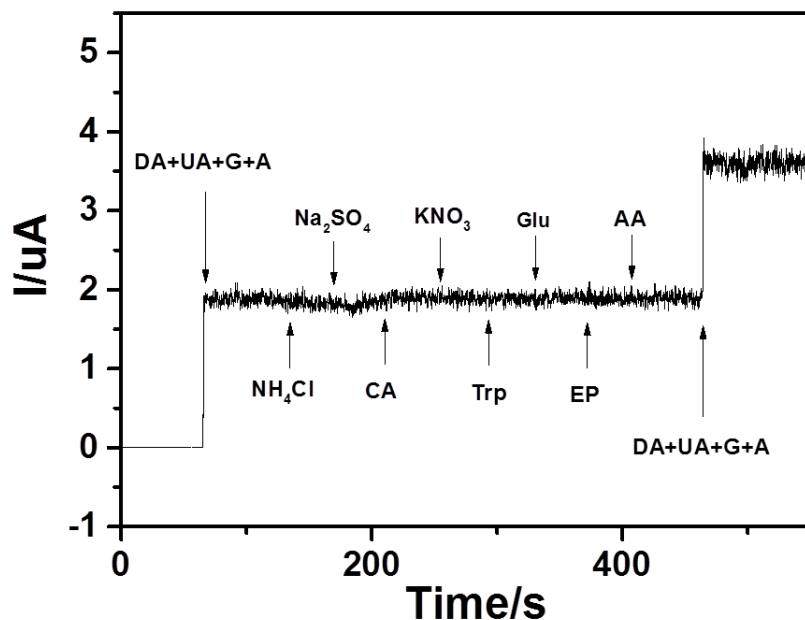


**Figure 13.** Chronoamperometry of a successively added mixture of 20  $\mu\text{M}$  DA, 20  $\mu\text{M}$  UA, 20  $\mu\text{M}$  G, 15  $\mu\text{M}$  A and potential disruptors containing 50 mM  $\text{NH}_4^+$ ,  $\text{Cl}^-$ ,  $\text{SO}_4^{2-}$ ,  $\text{NO}_3^-$ , 5 mM CA, Glu, Trp and 50  $\mu\text{M}$  EP, AA at 1.30 V on poly-Gly/GPE in PBS (pH 4.0).

### 3.6. Stability, repeatability and reproducibility

The current density of the four biomolecules within a month (stored in refrigerator) decreased by 6.7%, 6.1%, 1.1% and 1.8% compared to the original signals in PBS (pH 4.0). Thus, the proposed electrode had eminent stability after long-term storage.

Ten successive measurements to simultaneously discriminate the four biomolecules were performed using the identical poly-Gly/GPE, and their relative standard deviations (RSD) were less than 2.2%. Five different poly-Gly/GPEs were used to discriminate these four species, and their RSD were less than 6.9%. These data confirm that the as-prepared electrode was repeatable and reproducible.

### 3.7. Human serum analysis

The accuracy of the poly-Gly/GPE to detect the four species in human serum (pH 4.0) was evaluated by the standard addition method. The recovery rate was calculated by multiplying the ratio of theoretical concentration to actual concentration by 100% (Table 2).

**Table 2.** Human serum analysis.

Sample	Added ( $\mu\text{mol L}^{-1}$ )				Founded ( $\mu\text{mol L}^{-1}$ )				Recovery (%)			
	DA	UA	G	A	DA	UA	G	A	DA	UA	G	A
Serum 1	12.00	15.00	10.00	20.00	12.03	15.04	10.09	19.74	100.3	100.3	100.9	98.70
Serum 2	24.00	30.00	15.00	30.00	23.89	29.85	14.79	29.68	99.54	99.50	98.60	98.93
Serum 3	36.00	45.00	20.00	40.00	35.96	45.10	20.03	40.69	100.3	100.3	100.9	98.70

#### 4. CONCLUSIONS

A flexible poly-Gly/GPE was prepared by transferring a free-standing CVD graphene film to PET and electrodepositing Gly onto the surface of GPE. Due to the excellent catalytic activities of the proposed electrode, four sharp oxidation peaks were well separated to simultaneously detect the four biomolecules. The widths of linear ranges and low detection limits were obtained. This ultra-stable electrode can be directly used to discriminate the four biomolecules after long-term storage. In practical application, a promising strategy to selectively discriminate these four analytes in human serum was provided based on poly-Gly/GPE with outstanding anti-interference ability.

#### ACKNOWLEDGEMENT

This study was supported by the National Natural Science Foundation of China (No. 21575160).

#### References

1. R.M. Wightman, L.J. May and A.C. Michael, *Anal. Chem.*, 60 (1988) 769.
2. M. Velasco and A. Luchsinger, *Am. J. Ther.*, 5 (1998) 37.
3. W. Zhang, Y. Chai, R. Yuan, J. Han and S. Chen, *Sens. Actuator B-Chem.*, 183 (2013) 157.
4. X. Zheng, X. Zhou, X. Ji, R. Lin and W. Lin, *Sens. Actuator B-Chem.*, 178 (2013) 359.
5. L.Z. Zheng, S.G. Wu, X.Q. Lin, L. Nie and L. Rui, *Electroanalysis*, 13 (2001) 1351.
6. V.V. Dutt and H.A. Mottola, *Anal. Chem.*, 46 (1974) 1777.
7. C. Li, X. Qiu and Y. Ling, *J. Electroanal. Chem.*, 704 (2013) 44.
8. R.S. Sheng, F. Ni and T.M. Cotton, *Anal. Chem.*, 63 (1991) 437.
9. S. Shahrokhian, S. Rastgar, M.K. Amini and M. Adeli, *Bioelectrochemistry*, 86 (2012) 78.
10. S. Gao, H. Li, M. Li, C. Li, L. Qian and B. Yang, *J. Solid State Electrochem.*, 22 (2018) 3245.
11. S. He, P. He, X. Zhang, X. Zhang, K. Liu, L. Jia and F. Dong, *Anal. Chim. Acta*, 1031 (2018) 75.
12. X. Liu, L. Zhang, S. Wei, S. Chen, X. Ou and Q. Lu, *Biosens. Bioelectron.*, 57 (2014) 232.
13. L.M. Niu, K.Q. Lian, H.M. Shi, Y.B. Wu, W.J. Kang and S.Y. Bi, *Sens. Actuator B-Chem.*, 178 (2013) 10.
14. H. Li, X. Wang and Z. Yu, *J. Solid State Electrochem.*, 18 (2013) 105.
15. Z.-H. Sheng, X.-Q. Zheng, J.-Y. Xu, W.-J. Bao, F.-B. Wang and X.-H. Xia, *Biosens. Bioelectron.*, 1. 34 (2012) 125.
16. H. Yin, Y. Zhou, Q. Ma, S. Ai, P. Ju, L. Zhu and L. Lu, *Process Biochem.*, 45 (2010) 1707.
17. X. J. Zhao, H. Hou, X. T. Fan, Y. Wang, Y. M. Liu, C. Tang, S. H. Liu, P. P. Ding, J. Cheng, D. H. Lin, C. Wang, Y. Yang and Y. Z. Tan, *Nat. Commun.*, 10 (2019) 3057.
18. C. Liu, Z. Yu, D. Neff, A. Zhamu and B.Z. Jang, *Nano Lett.*, 10 (2010) 4863.

19. S. Guo and S. Dong, *Chem. Soc. Rev.*, 40 (2011) 2644.
20. K.S. Novoselov, A.K. Geim, S.V. Morozov, D. Jiang, Y. Zhang, S.V. Dubonos, I.V. Grigorieva and A.A. Firsov, *Science*, 306 (2004) 666.
21. N. Leconte, H. Kim, H. J. Kim, D. H. Ha, K. Watanabe, T. Taniguchi, J. Jung and S. Jung, *Nanoscale*, 9 (2017) 6041.
22. K.S. Novoselov, V.I. Fal'ko, L. Colombo, P.R. Gellert, M.G. Schwab and K. Kim, *Nature*, 490 (2012) 192.
23. B. Deng, Z. Liu and H. Peng, *Adv. Mater.*, 31 (2019) 1800996.
24. D. He, P. Zhang, S. Li and H. Luo, *J. Electroanal. Chem.*, 823 (2018) 678.
25. D.A.C. Brownson and C.E. Banks, *Phys. Chem. Chem. Phys.*, 14 (2012) 8264.
26. K. Li, J. Jiang, Z. Dong, H. Luo and L. Qu, *Chem. Commun.*, 51 (2015) 8765.
27. J. Jiang, P. Zhang, Y. Liu and H. Luo, *Anal. Methods*, 9 (2017) 2205.
28. D. He, S. Li, P. Zhang and H. Luo, *Anal. Methods*, 9 (2017) 6689.
29. Y. Luo, Y. Zhang, L. Lu and H. Luo, *J. Electroanal. Chem.*, 856 (2020) 113737.
30. J.W. Suk, A. Kitt, C.W. Magnuson, Y. Hao, S. Ahmed, J. An, A.K. Swan, B.B. Goldberg and R.S. Ruoff, *ACS Nano*, 5 (2011) 6916.
31. J. Kang, D. Shin, S. Bae and B.H. Hong, *Nanoscale*, 4 (2012) 5527.
32. E. J. Heller, Y. Yang, L. Kocia, W. Chen, S. Fang, M. Borunda and E. Kaxiras, *ACS Nano*, 10 (2016) 2803.
33. Z. Sun, Z. Yan, J. Yao, E. Beitler, Y. Zhu and J.M. Tour, *Nature*, 468 (2010) 549.
34. M.S. Dresselhaus, A. Jorio, M. Hofmann, G. Dresselhaus and R. Saito, *Nano Lett.*, 10 (2010) 751.
35. R. Bowling, R.T. Packard and R.L. McCreery, *Langmuir*, 5 (1989) 683.
36. K. Aoki, K. Akimoto, K. Tokuda, H. Matsuda and J. Osteryoung, *J. Electroanal. Chem.*, 171 (1984) 219.
37. E. Laviron, *J. Electroanal. Chem.*, 101 (1979) 19.
38. W. He, W. Zhang, L. Zhang, X. Zhang and F. Yang, *J. Electroanal. Chem.*, 797 (2017) 61.
39. W. He, Y. Ding, L. Ji, X. Zhang and F. Yang, *Sens. Actuator B-Chem.*, 241 (2017) 949
40. H. Li, X. Wang and Z. Yu, *J. Solid State Electrochem.*, 18 (2013) 105.
41. D. Gao, M. Li, H. Li, C. Li, N. Zhu and B. Yang, *J. Solid State Electrochem.*, 21 (2016) 813.
42. T. Gan, Z. Wang, Z. Shi, D. Zheng, J. Sun and Y. Liu, *Biosens. Bioelectron.*, 112 (2018) 23.
43. S. Pradhan, S. Pramanik, D. K. Das, R. Bhar, R. Bandyopadhyay, P. Millner and P. Pramanik, *New J. Chem.*, 43 (2019) 10590.
44. Z. Lu, Z. Shi, S. Huang, R. Zhang, G. Li and Y. Hu, *Talanta*, 214 (2020) 120864.